

# RSC Advances



This is an *Accepted Manuscript*, which has been through the Royal Society of Chemistry peer review process and has been accepted for publication.

*Accepted Manuscripts* are published online shortly after acceptance, before technical editing, formatting and proof reading. Using this free service, authors can make their results available to the community, in citable form, before we publish the edited article. This *Accepted Manuscript* will be replaced by the edited, formatted and paginated article as soon as this is available.

You can find more information about *Accepted Manuscripts* in the [Information for Authors](#).

Please note that technical editing may introduce minor changes to the text and/or graphics, which may alter content. The journal's standard [Terms & Conditions](#) and the [Ethical guidelines](#) still apply. In no event shall the Royal Society of Chemistry be held responsible for any errors or omissions in this *Accepted Manuscript* or any consequences arising from the use of any information it contains.

Cite this: DOI: 10.1039/coxx00000x

www.rsc.org/xxxxxx

ARTICLE TYPE

## Low-Temperature Solution-processed Zn-doped SnO<sub>2</sub> Photoanodes: Enhancements in Charge Collection Efficiency and Mobility†

Sambhaji S. Bhande,<sup>a</sup> Dipak V. Shinde,<sup>b</sup> Shoyeb Mohamad F. Shaikh,<sup>c</sup> Swapnil B. Ambade,<sup>d</sup> Rohan B. Ambade,<sup>d</sup> Rajaram S. Mane,<sup>a, b,\*</sup> Inamuddin,<sup>e</sup> Mu. Naushad,<sup>f</sup> and Sung-Hwan Han<sup>a,\*</sup>

Received (in XXX, XXX) Xth XXXXXXXXX 20XX, Accepted Xth XXXXXXXXX 20XX

DOI: 10.1039/b000000x

Increase in charge collection efficiency and charge mobility from 78 to 89% and 0.02 to 0.04 cm<sup>2</sup> V<sup>-1</sup> s<sup>-1</sup>, respectively, in low-temperature solution-processed Zn-doped SnO<sub>2</sub> photoanodes resulted into two-fold enhancement in power conversion efficiency (PCE) as compared to Zn free SnO<sub>2</sub> photoanodes in the dye-sensitized solar cells (DSSCs).

DSSCs have attracted immense interest as promising candidates for the future development of commercially viable solar cells.<sup>1-3</sup> Nanocrystalline TiO<sub>2</sub>, ZnO, Nb<sub>2</sub>O<sub>5</sub>, WO<sub>3</sub> and SnO<sub>2</sub> have widely been envisaged as photoanodes for developing high performance DSSCs to obtain the balance between the cost and ease of fabrication, compared with Si-based solar cells.<sup>4</sup> As a DSSC photoanode, TiO<sub>2</sub> has been a dominant material that consistently exhibits PCE as high as ~12%.<sup>5</sup> Analogous to TiO<sub>2</sub>, ZnO has also been explored largely due to its similar band gap energy (E<sub>g</sub> = 3.2 eV) and electronic energy levels. While, high electron mobility (μ) of ZnO (>200 cm<sup>2</sup> V<sup>-1</sup> S<sup>-1</sup>) is certainly an advantage, however, its instability in acidic electrolytes, restricts the electron injection rate from the sensitizer (dye) to ZnO by forming an insulating surface agglomerative layer.<sup>6</sup> Another chemically stable alternative, SnO<sub>2</sub> also possesses higher μ (~100–200 cm<sup>2</sup> V<sup>-1</sup> s<sup>-1</sup>) compared to TiO<sub>2</sub> (~10<sup>-2</sup> cm<sup>2</sup> V<sup>-1</sup> S<sup>-1</sup>).<sup>7</sup> However, one major disadvantage with SnO<sub>2</sub>-based DSSCs is its tendency to exhibit lower open circuit voltage (V<sub>oc</sub>). SnO<sub>2</sub>-based DSSCs is its tendency to exhibit lower open circuit voltage (V<sub>oc</sub>). This is due to

its 300 mV positively located conduction band level.<sup>8</sup> The inferior photovoltaic properties of SnO<sub>2</sub> are additionally attributed to faster electron recombination kinetics and poor dye uptake associated with the low isoelectric point.<sup>9</sup> Grätzel *et al.*,<sup>10</sup> demonstrated a significant improvement in photovoltaic parameters by covering the mesoporous SnO<sub>2</sub> with a thin shell of ZnO. Nevertheless, this chemically unstable component (ZnO) in the composite is a challenging issue that needs to be resolved. Previously, we reported that employing dual photosensitization can effectively suppress agglomeration of ZnO nanoparticles.<sup>11</sup> Thus, the most significant challenge is to complement the advantages of the present photoanode materials to construct a compound structure that is chemically stable and possesses higher charge collection kinetics for efficient PCE in DSSCs. In this context, the chemically stable Zn-doped SnO<sub>2</sub> can be a good alternative since the effective ionic radii of Zn<sup>2+</sup> (74 pm) is close to Sn<sup>4+</sup> (69 pm) and thus, it is expected that Zn<sup>2+</sup> ions can easily be incorporated into the lattice of SnO<sub>2</sub> to offer fascinating electronic properties collectively. Moreover, the Zn-doped films exhibit an elevated electron Fermi level, which may enhance band bending to lower the density of empty trap states.<sup>12</sup>

In this communication, we present a remarkable 2 fold enhancement in the photovoltaic performance of DSSCs containing chemically synthesized upright-standing Zn-doped SnO<sub>2</sub> nanoplates as photoanodes that exhibit high charge collection efficiency and dramatically reduced charge transport resistance than Zn-free SnO<sub>2</sub> photoanode with impressive overall PCE of 4.87%. The obtained PCE is by far the highest for low temperature chemically synthesized SnO<sub>2</sub>-based DSSCs.<sup>13</sup> This work is in continuation with our research focus on low temperature chemical synthesis of DSSC photoanodes.<sup>14</sup> Low temperature chemical synthesis route is extremely advantageous as it paves opportunities for facile and commercially viable scalable synthesis. Various Zn-doped SnO<sub>2</sub> photoanodes were synthesized using a simple chemical bath deposition method at 70 °C and termed as A~E with increasing Zn-doping concentration at successive interval of 1 wt.% starting from 0 wt.% for A and 4 wt.% Zn-doping for photoanode E. Detailed synthesis procedure is discussed in ESI†. The XRD spectra (Fig. 1) of all photoanodes confirm the tetragonal rutile structure of SnO<sub>2</sub> (File: 41-1445).

<sup>a</sup>Centre for Nanomaterials & Energy Devices, School of Physical Sciences, SRTM University, 431606, Nanded, India Email: [rsmene\\_2000@yahoo.com](mailto:rsmene_2000@yahoo.com), <sup>b</sup>Department of Chemistry, Hanyang University, Seongdong-gu, 133791 Seoul, Korea Email: [shhan@hanyang.ac.kr](mailto:shhan@hanyang.ac.kr), <sup>c</sup>Clean Energy Research Center, Korea Institute of Science and Technology, Seoul 130-650, Korea, <sup>d</sup>School of semiconductor and Chemical Engineering, Chonbuk national university, Duckjin-dong 664-14, Jeonju 561-756, Korea, <sup>e</sup>Department of Applied Chemistry, Faculty of Engineering and Technology, Aligarh Muslim University, Aligarh –202002, India, <sup>f</sup>Department of Chemistry, College of Science, Building 5, King Saud University, Riyadh, Saudi Arabia.

†Electronic Supplementary Information (ESI) available: Experimental procedures with structural characterizations and supplementary figures (Fig. S1-S6) in addition to tables (T1-T4).

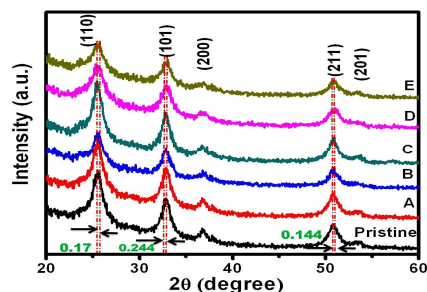


Fig. 1 XRD spectra of pristine and Zn-doped SnO<sub>2</sub> nanoplates.

For Zn-doped SnO<sub>2</sub> photoanodes, no other crystalline phase and peaks of impurities were detected (Fig. 1, spectra A–E), indicating neither separate SnO<sub>2</sub>/ZnO nor Zn<sub>x</sub>Sn<sub>1-x</sub>O<sub>2</sub> composite structure has been formed. To investigate the effect of Zn<sup>2+</sup> ion doping on the crystallinity of SnO<sub>2</sub>, (110), (200), and (211) diffraction peaks are monitored. Spectra (B–E) of Fig. 1 reveal that, with increase in Zn wt. %, the 2θ values shift by 0.17, 0.244 and 0.144 degrees, respectively, compared to that of pristine SnO<sub>2</sub>. This clearly proves that Zn<sup>2+</sup> ion incorporation has led to a lattice deformation in the Zn-doped SnO<sub>2</sub>. Moreover, on Zn-doping, the photoelectron peaks for Sn 3d<sub>5/2</sub> and Sn 3d<sub>3/2</sub> in the X-ray photoelectron spectroscopy (XPS) spectra (Fig. S2b, ESI†) appears to have decreased from 487.96 eV to 486.02 eV and 497 eV to 494.97 eV, respectively. The O1s transition peak (Fig. S2c, ESI†) is shifted towards the lower binding energy by 2.01 eV from 531.98 eV to 529.97 eV. Also, the strong Zn 2p<sub>3/2</sub> peak (Fig. S2d, ESI†) at binding energy of 1056 eV further confirms the presence of Zn in the SnO<sub>2</sub> matrix.

The FE-SEM images of pristine and 0–4 wt% Zn-doped SnO<sub>2</sub> photoanodes (Fig. 2), reveal clear change in the parent surface morphology after Zn-doping. The width of individual pristine nanosheet was found to be 15–20 nm that increased to 30–60 nm for Zn-doping of 0–4 wt%. This suggests that Zn-doping makes significant change in the morphology of parent nanostructure (Fig. 2a); with distinct change in roughness with increasing Zn concentration (Fig. 2 b–d). It is expected that the newly formed rough structures must aid in superior dye adsorption. This interconnected network of nanoplates should offer mechanical strength along with rapid electron transport pathways due to the minimized grain boundaries. With further increase in Zn concentration above 3 wt. %, the nanoplates tend to bend. This may be due to the lower mechanical strength of upright standing SnO<sub>2</sub> nanoplates developed due to breaking of bonds after excessive Zn incorporation.

Fig. 3a shows the *J-V* characteristics of DSSCs (fabricated as per structure depicted in Fig. 3a) for pristine and Zn-doped SnO<sub>2</sub> photoanodes. It is observed that Zn doping of SnO<sub>2</sub> has significant impact on DSSCs performance. The detailed photovoltaic parameters are summarized in Table 1 (ESI†). DSSCs comprising pristine SnO<sub>2</sub> photoanode exhibited short-circuit current density (*J*<sub>sc</sub>) of 6.73 mA/cm<sup>2</sup>, *V*<sub>oc</sub> of 0.55V and a fill factor (*ff*) of 0.51 which itself is an improvement from our previously reported PCE of 0.37% for pristine SnO<sub>2</sub> photoanode sensitized with dye.<sup>13b</sup> However PCE increased to 2.54% after TiCl<sub>4</sub> treatment because of pronounced increase in *J*<sub>sc</sub> and *V*<sub>OC</sub> although the *ff* dropped. This is attributed to the increase in

roughness induced by TiCl<sub>4</sub> treatment that eventually increased the uptake of dye and decreased the electron/electrolyte recombination.<sup>15</sup>

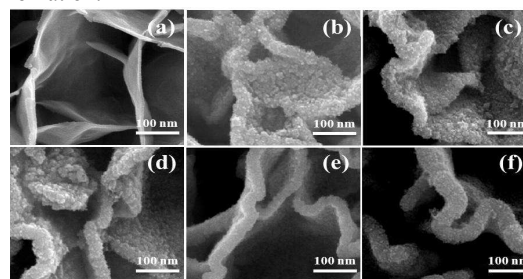


Fig. 2 FE-SEM images of (a) pristine SnO<sub>2</sub>, (b) after TiCl<sub>4</sub> surface treatment, and (c–f) 1–4wt% Zn-doped SnO<sub>2</sub> photoanodes.

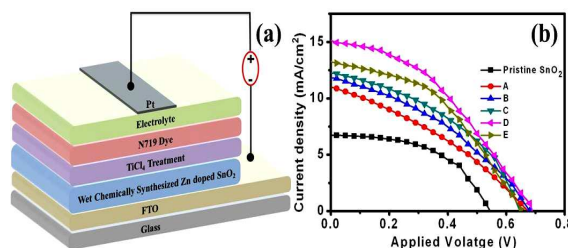
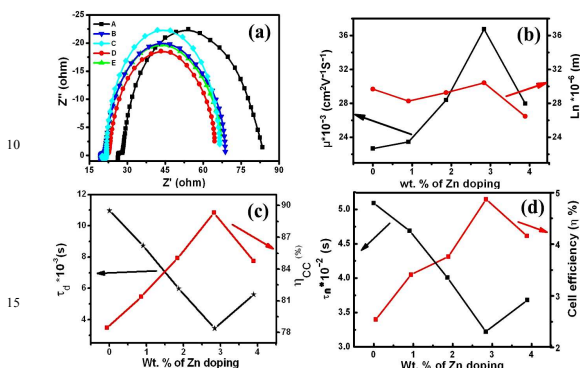


Fig. 3 (a) Device structure and, (b) *J-V* curves of all DSSCs under 1 sun illumination.

In DSSCs of Zn-doped SnO<sub>2</sub> photoanodes, an exponential increase in photovoltaic performance with Zn doping level up to 3 wt. % is observed. A maximum PCE of 4.87% is achieved for DSSCs having 3 wt. % of Zn-doped SnO<sub>2</sub> photoanode, which is about two times higher than DSSCs of pristine SnO<sub>2</sub> photoanode. Increased photovoltaic performance is majorly due to enhancement in *J*<sub>sc</sub>. This is attributed to enhanced charge-generation efficiency; suppressed electron recombination (explained later using EIS analyses), and higher dye loading, compared to pristine SnO<sub>2</sub> photoanode.<sup>16</sup> For comparison, DSSCs results of SnO<sub>2</sub> photoanodes synthesized using other methods are given in Table 4 of ESI†. Incident photon-to-electron conversion efficiencies (IPCE) of pristine and Zn-doped SnO<sub>2</sub> photoanodes were measured (ESI† S5). Considerable change in IPCE measurements after TiCl<sub>4</sub> treated is obtained which in fact is significantly less compared to wet chemically synthesized SnO<sub>2</sub>-TiCl<sub>4</sub>.<sup>13b</sup> However, with Zn-doping IPCE values and wavelength range are substantially increased. The IPCE number is increased from 30% to 56% (nearly double) which is just due to Zn-doping effect, consistent to *J-V* measurements. Decrease in IPCE at higher Zn-doping level is due to negative mass/agglomeration effect of ZnO with SnO<sub>2</sub>.<sup>17</sup>

A UV-*vis* spectroscopy investigation, as shown in Fig. S4 (ESI†), revealed a proportionally higher increase in the optical density at higher wavelengths, strongly indicating increased dye loading after Zn-doping. The dye-loading experiments revealed that the dye loading increased by 152 and 350 % respectively, for pristine and 3wt. % Zn-doped SnO<sub>2</sub>. The suppressed electron recombination is evident from the *J-V* spectra of DSSCs measured under forward bias potential in dark as shown in Fig. S3 (ESI†). The dark current onset of a pristine SnO<sub>2</sub> photoanode occurred at low forward bias, indicating faster electron-

recombination kinetics.<sup>18</sup> In order to analyze the electron transport behavior in the DSSCs, the electrochemical impedance spectroscopy (EIS) measurements were performed, which distinguishes the charge transport resistance ( $R_{ct}$ ) and chemical capacitance of the device.



**Fig. 4** (a) Nyquist plots, dependence of (b) electron mobility and diffusion length, (c) charge collection efficiency and transit time and (d) electron life time and cell efficiency with Zn- doping.

The equivalent circuit used for EIS measurements and EIS data with electronic parameters are presented in Fig. S6 and Table 3 (ESI†). The Nyquist plots shown in Fig. 4a measured under 1 sun conditions for all DSSCs at respective  $V_{oc}$  condition clearly reveal lower  $R_{ct}$  for the 3 wt. % Zn-doped  $\text{SnO}_2$  photoanode, resulting due to the reduction of trap states for photogenerated electrons. The EIS measurements revealed higher  $\mu$  for Zn-doped photoanodes than the pristine one indicating favorable electron transport through a longer distance with less diffusive hindrance after Zn-doping. The variation of diffusion length ( $L_n$ ) and  $\mu$  with respect to Zn doping is presented in Fig. 4(b). Further increase in  $\text{Zn}^{2+}$  ion concentration above 3 wt. % in solution starts deceleration in  $L_n$  value. This is accomplished with significant increase in number of bond deformation and generation of more trap states within the photoanode.<sup>19</sup> The trend of increasing  $\mu$  value (Table 3, ESI†) with Zn intercalation in  $\text{SnO}_2$  matrix is clearly noticed (from  $0.022 \text{ cm}^2 \text{ V}^{-1} \text{ s}^{-1}$  to  $0.04 \text{ cm}^2 \text{ V}^{-1} \text{ s}^{-1}$  for pristine and 3 wt. % Zn-doped  $\text{SnO}_2$  photoanodes, respectively). Zn-doping also resulted in the decrease in electron transit time ( $\tau_d$ ) (Fig. 4c) from 0.01 to 0.06 s for pristine and 3 wt. % Zn-doped  $\text{SnO}_2$  photoanodes, respectively. The decrease in  $\tau_d$  proved minimization of the trapping states; facilitating the effective transport of photogenerated electrons. The mean electron lifetime ( $\tau_n$ ) calculated in all DSSCs using EIS is presented in Table S3, ESI†. Fig. 4(d) represents the plot of variation of  $\tau_n$  and PCE of the DSSCs with varying Zn-doping concentration. The  $\tau_n$  of doped photoanode is smaller than that for undoped photoanode. However, with Zn-doping, the  $\tau_n$  values are nearly one order of magnitude greater than their corresponding  $\tau_d$  values justifying that Zn-doping can minimize the trapping–detrapping processes. The charge collection efficiency ( $\eta_{cc}$ ) is found to increase from 78.45% to 89.32% for undoped and 3 wt. % Zn-doped  $\text{SnO}_2$  photoanodes. With further increase of Zn-doping,  $\eta_{cc}$  is reduced to 84.76% and  $\tau_d$  increased to 0.06s.

In summary, a low-temperature (70 °C) wet chemical solution method was carried out for the synthesis of Zn-doped

$\text{SnO}_2$  photoanodes. DSSCs fabricated with photoanodes of optimized Zn-doping (3 wt. %) exhibited an overall PCE of 4.87 % and IPCE of 56%, that is two-fold higher than the undoped  $\text{SnO}_2$  photoanodes. The shortening of electron transit time after Zn-doping and increased charge collection efficiency proved to be advantageous for the high performance obtained in this work.

This research was financially supported by; a) University Grant Commission, Delhi India through project F.41-844/2012 (SR) and b) King Saud University, Deanship of Scientific Research, College of Science Research Center.

## Notes and references

- B. O'Regan and M. Grätzel, *Nature*, 1991, **353**, 737.
- P. Wang, S. M. Zakeeruddin, J. E. Moser, M. K. Nazeeruddin, T. Sekiguchi and M. Grätzel, *Nat. Mater.*, 2003, **2**, 402.
- F. Sauvage, F. Di Fonzo, A. L. Bassi, C. S. Casari, V. Russo, G. Divitini, C. Ducati, C. E. Bottani, P. Comte and M. Grätzel, *Nano. Lett.*, 2010, **10**, 2562.
- Y. C. Qiu, W. Chen and S. H. Yang, *Angew. Chem., Int. Ed.*, 2010, **49**, 3675.
- A. Yella, H-W Lee, H. N. Tsao, C. Yi, A. K. Chandiran, Md. K. Nazeeruddin, E. W-G. Diao, C-Y Yeh, S. M. Zakeeruddin, M. Grätzel, *Science*, 2011, **334**, 629.
- Q. F. Zhang, C. S. Dandaneau, X. Y. Zhou and G. Z. Cao, *Adv. Mater.*, 2009, **21**, 4087.
- M. S. Arnold, P. Avouris, Z. W. Pan and Z. L. Wang, *J. Phys. Chem. B*, 2002, **107**, 659.
- S. S. Bhande, G. A. Taur, A. V. Shaikh, O-S Joo, M-M Sung, R. S. Mane, A. V. Ghule, S-H. Han, *Mater. Lett.*, 2012, **79**, 29.
- A. Kloke, F. von Stetten, R. Zengerle, S. Kerzenmacher, *Adv. Mater.* 2011, **23**, 4976.
- A. Kay and M. Grätzel, *Chem. Mater.*, 2002, **14**, 2930.
- T. Ganesh, R. S. Mane, G. Cai, J.-H. Chang, S.-H. Han, *J. Phys. Chem. C*, 2009, **113**, 7666.
- K.-P. Wang, H. Teng, *Phys. Chem. Chem. Phys.*, 2009, **11**, 9489.
- a) D. V. Shinde, I. Lim, C. S. Kim, J. K. Lee, R. S. Mane and S. H. Han, *Chem. Phys. Lett.*, 2012, **542**, 66, b) D. V. Shinde, R. S. Mane, I.-H. Oh, J. K. Lee, S.-H. Han, *Dalton Trans.*, 2012, **41**, 10161.
- S. B. Ambade, R. B. Ambade, R. S. Mane, G-W. Lee, S. Md. F. Shaikh, S. A. Patil, O-S. Joo, S-H. Han and S-H. Lee, *Chem. Comm.*, 2013, **49**, 2921.
- B. C. O'Regan, J. R. Durrant, P. M. Sommeling and N. G. Bakker, *J. Phys. Chem. C*, 2007, **111**, 14001.
- H. J. Snaith and C. Ducati, *Nano Lett.*, 2010, **10**, 1259.
- a) S. B. Ambade, R.S. Mane A. V. Ghule, M. G. Takawale, A. Abhyankar, B. Cho, *Scripta Materilia*, 2009, **61**, 12-15. b) R. S. Mane, W. J. Lee, H. M. Pathan and S. H. Han, *J. Phys. Chem. B* 2005, **109**, 24254.
- S. Ito, P. Liska, P. Comte, R. Charvet, P. Pechy, U. Bach, L. Schmidt-Mende, S. M. Zakeeruddin, A. Kay, M. K. Nazeeruddin and M. Grätzel, *Chem. Commun.*, 2005, **34**, 4351.
- P. Sun, L. You, Y. Sun, N. Chen, X. Li, H. Sun, J. Ma and G. Lu, *Cryst. Eng. Commun.*, 2012, **14**, 1701-1708.